SAND2013-10345C

Tribrachial, tetrabrachial and pentabrachial structures in dimethyl ether edge-flames at NTC conditions

Nominated colloquium: laminar flames
Word count: 5,729 (method 2)
Main text: 4003 words, References: 540 words, Figure 1: 114 words, Figure 2: 97 words, Figure 3: 365 words, Figure 4: 253 words, Figure 5: 194 words, Table 1: 64 words, Table 2: 99 words
Print in colour: no

Alex Krisman[a,*], Evatt R. Hawkes[a,b], Mohsen Talei[a], Ankit Bhagatwala[c], Jaqueline H. Chen[c]

[a] *School of Mechanical and Manufacturing Engineering, The University of New South Wales, Sydney, NSW 2052, Australia*
[b] *School of Photovoltaic and Renewable Energy Engineering, The University of New South Wales, Sydney, NSW 2052, Australia*
[c] *Combustion Research Facility, Sandia National Laboratories, Livermore, CA 96551-0969, USA*

Abstract

The structure and stabilisation mechanism of partially premixed, laminar, dimethyl ether (DME) flames are investigated using two-dimensional direct numerical simulation (DNS). The simulations are performed at a pressure of 40 atmospheres and at oxidiser temperatures above the ignition temperature of 700, 900, 1100, 1300, and 1500 K, while keeping the lift-off length approximately fixed by varying the inlet velocity. DME exhibits two stage ignition below approximately 1100 K and a negative temperature coefficient (NTC) regime from approximately 800 to 1100 K. The DNS results are investigated by considering the thermochemical structure of the flames and by applying a transport budget analysis to key chemical species. The results show a transition from a lifted flame stabilised by propagation to a flame stabilised by autoignition with increasing temperature. At 700 K, the flame has a classical tribrachial structure similar to freely propagating edge flames at non-autoignitive conditions. The intermediate temperature cases reveal a complex transition involving multiple heat release pathways *upstream* of the stabilisation point. At 900 K, the flame consists of a main-tribrachial structure and an additional upstream branch due to low temperature chemistry: this is termed a tetrabrachial flame. At 1100 and 1300 K, two upstream branches are observed in addition to the main tribrachial structure, one due to low temperature chemistry and the other due to high temperature chemistry, which initiates autoignition and stabilises the flame:

*Corresponding author
Email address: a.krisman@unsw.edu.au (Alex Krisman)

these are termed pentabrachial flames. At 1500 K, the low temperature upstream branch is suppressed, so there is only one upstream branch due to high temperature chemistry which proceeds to autoignition, this flame has a tetrabrachial structure, but one which is different from that observed in the 900 K cases.
Keywords:

dimethyl ether, tribrachial flame, triple flame, negative temperature coefficient, autoignition

---

1. Introduction

Many combustion devices, such as diesel engines, staged gas-turbines for power generation, and many industrial burners operate in a partially premixed combustion mode. The combustion of partially premixed reactants often involves a leading edge-flame. As discussed by Buckmaster [1], an edge flame is fundamentally a two-dimensional structure. At non-autoignitive conditions, and for sufficiently low mixture-fraction gradients, the leading edge is a crescent-shaped premixed flame, propagating approximately normal to the mixture fraction gradient, that is composed of lean and rich branches. Behind the leading premixed edge, there is a nonpremixed flame centred on the stoichiometric mixture fraction which consumes the partially oxidised fuel from the rich premixed branch and the excess oxygen from the lean premixed branch. The nonpremixed, lean premixed, and rich premixed branches coincide at the leading edge of the flame which is also called the triple point. In this situation the edge flame is also referred to as a triple flame or tribrachial flame for its three branches.

Many numerical and experimental studies have been conducted to investigate edge flames in non-autoignitive conditions, as reviewed by Chung [2]. The bulk of the literature has focused on characterising effects such as premixedness [3–6], strain [7–9], and differential diffusion [4, 10] on the propagation and stabilisation of tribrachial flames.

One important application of partially premixed combustion is the diesel engine. In diesel engines, fuel is injected in to the cylinder at high velocity in a high temperature environment, and once ignited, a lifted flame is established. The mechanism of flame stabilisation in diesel engines, which determines the lifted height and thus emissions [11] , is still debated. It is possible that edge flames are involved, however it is clear that such edge flames could be different from conventional edge flames observed in atmospheric conditions due to the influence of autoignition. Despite this potential importance, no detailed numerical studies of edge flames have been conducted at nominal engine pressures and temperatures, or using a fuel capable of reproducing even the qualitative features of the complex chemical behaviours of diesel fuel. These chemical behaviours include two stage autoignition, cool-flame chemistry and the negative temperature coefficient (NTC) regime, *e.g.* [12, 13].

The objective of this study is to investigate dimethyl ethere stabilised lifted flames in a heated autoignitive mixture, similar to diesel lift-off stabilisation. In the present study a dimethyl ether (DME) fuel jet at a pressure of 40 atmospheres and a temperature range of 700 to 1500 K is simulated. DME has been selected mainly because it exhibits two stage ignition and a NTC regime while still being a relatively simple

bio-alcohol molecule for which a moderately sized kinetic mechanism has been developed. At a pressure of 40 atmospheres, dimethyl ether exhibits two stage ignition and a NTC regime from approximately 800 to 1100 K, so the variation of oxidiser temperature considered here is appropriately selected to investigate the interaction of complex chemistry with a spatially developing partially premixed flame.

Direct numerical simulations (DNS) are performed in two-dimensional, spatially developing mixing layers with various oxidiser temperatures that span the NTC regime. The DNS are then analysed to understand the resulting flame structures.

2. Numerical Method and Flow Parameters

The DNS are performed using the massively parallel DNS code S3D [14], which solves the compressible Navier-Stokes, conservation of mass, energy, and species mass fraction equations for a reactive flow.

The computational domain is spatially two-dimensional in the streamwise, $\hat{x}$, and cross-stream, $\hat{y}$, directions. A fixed, uniform streamwise velocity component U is imposed at the lower $\hat{x}$ boundary, while the transverse velocity is set to zero. The domain is initialised with a mixing layer between pure oxidiser and pure fuel that is defined using a hyperbolic tangent profile of mixture fraction, Z, in the y direction, centered about the location y=-0.3mm. The fuel is composed of 70% DME and 30% N_2 by volume and has a constant temperature of 400 K. The oxidiser is comprised of 21% O_2 and 79% N_2 by volume. The width of the mixing layer is determined by σ and is fixed at 0.2 mm. The temperature profile is determined by the mixture fraction and the fuel and oxidiser temperatures by assuming an adiabatic mixing process. The size of the domain is fixed at 3 mm in the $\hat{x}$ direction and 1.5 mm in the $\hat{y}$ direction.

The left $\hat{y}$ boundary and upper $\hat{x}$ boundary are non-reflecting outflows evaluated with the Navier-Stokes characteristic boundary condition method [15]. The right $\hat{y}$ boundary imposes a symmetry condition at y=0. The mesh is structured and Cartesian. Spatial gradients are evaluated using eight-order central differencing scheme and time advancement employs a fourth-order, six-stage explicit Runge-Kutta method. S3D has been used for a number of other studies of laminar and turbulent flames [16–21]. Due to the high pressure, a very fine grid resolution, $\Delta x = 0.7$ microns, was required to resolve all of the species mass fraction profiles. The fine grid resolution implied a very small timestep, $\Delta t = 0.5$ ns. The Δx and Δt values were deemed to be sufficient as judged by a grid independence test (not shown here).

The five cases considered are distinguished by oxidiser temperature and inlet velocity. As the oxidiser temperature is varied, the inlet velocity is adjusted to maintain a near-constant lift-off length. Table 1

lists the oxidiser temperature and inlet velocity for each case.

The chemical mechanism is a 30 species reduced mechanism provided by Lu et al. (personal communication) [22]. The mechanism was obtained by a reduction of the mechanism developed by Zhao *et al.* [23] using reduction methods outlined by Lu and Law [24]. A mixture-averaged molecular transport model was employed [14].

Figure 1 compares the first and second stage ignition delay times for the detailed and reduced mechanisms. The first stage ignition delay times of the reduced mechanism are slightly over-predicted, but within 15% of the values for the detailed mechanism. The two stage ignition region is very well matched. The most prominent discrepency is the over-prediction of the main ignition delay times in the NTC region. The over-prediction is within 25% and does not significantly affect the location or range of the NTC region. Given that this study is focussing on investigating the qualitative features of two stage ignition and NTC behaviour, this level of agreement is deemed suffcient.

3. Dimethyl ether

To provide the necessary background to explain the DNS results, the basic ignition characteristics are first outlined. As previously explained [23, 25–27] DME is a fuel that has temperature dependent ignition characteristics. At high oxidiser temperatures (above approximately 1100 K for a stochiometric mixture at 40 atm), ignition occurs in a single stage wherein fuel molecules break down rapidly by unimolecular decomposition, radical attack and beta-scission leading to chain branching and thermal runaway. At lower temperatures (below approximately 1100 K for a stoichiometric mixture at 40 atm), ignition occurs in two stages with distinct peaks of heat release rate. The first stage is controlled by competing, low temperature chemical pathways, and the second stage involves rapid, thermal dissociation and oxidation of the remaining fuel and intermediate species produced from the first stage of ignition.

At low temperatures (below 1100 K for a stochiometric mixture at 40atm) oxidation of DME is initiated by hydrogen abstraction (R1). The resulting CH_3OCH_2 species can then undergo oxygen addition (R2). Methoxymethyl-peroxy radicals ($CH_3OCH_2O_2$) subsequently undergoe internal H abstraction (isomerisation) (R3) [25, 27].

$$CH_3OCH_3 + R \longrightarrow CH_3O\dot{C}H_2 + R{-}H \tag{R1}$$

$$CH_3O\dot{C}H_2 + O_2 \longleftrightarrow CH_3OCH_2\dot{O}_2 \tag{R2}$$

$$CH_3OCH_2\dot{O}_2 \longleftrightarrow \dot{C}H_2OCH_2O_2H \tag{R3}$$

Methoxymethyl-hydroperoxide ($\dot{C}H_2OCH_2O_2H$) then either undergoes another oxygen addition step (R4) which leads to chain branching reaction or a beta-scission process (R5) which produces two stable formaldehyde molecules and only one OH, and hence is a chain propagating process [25, 27].

$$\dot{C}H_2OCH_2O_2H + O_2 \longleftrightarrow \dot{O}_2CH_2OCH_2O_2H \tag{R4}$$

$$\dot{C}H_2OCH_2O_2H \longrightarrow 2\,CH_2O + \dot{O}H \tag{R5}$$

At low temperatures (R2) and (R4) favour the forward direction, leading to chain branching and heat release. The temperature rise caused by the chain branching reactions results in the reverse rates of (R2) and (R4) increasing due to the temperature dependence of these reactions [27]. This leads to a reduction in the reactivity of the system. Additionally, the elevated temperature favours the propagating (R4) reaction. These factors lead to the termination of the first stage. After the low temperature heat release (from the first stage of ignition) is suppressed by the increased system temperature, the thermal decomposition of species CH_3OCH_2 gradually increases via beta-scission. This leads to a slow build-up of radicals which attack the remaining fuel and intermediate species which eventually proceeds to a rapid thermal runaway associated with high temperature chemistry (i.e. second stage of ignition).

For transitional temperatures, between about 800 K and 1100K at a pressure of 40 atmospheres, DME exhibits a NTC regime in which ignition delay time increases with increasing temperature (for stoichiometric mixture fraction). Two stage ignition also occurs in the NTC regime. The NTC behaviour is manifested by the temperature dependence of reaction (R4) [27]. The equilibrium of this reaction shifts towards the reactants at higher temperatures, and this accounts for the negative temperature coefficient. With increasing T_{ox} in the NTC regime there is less low temperature heat release and the duration between the first and main stage of ignition is therefore also longer.

For cases that undergo two stage ignition, we define the first ignition delay time, τ_1, as the timing of the the first peak in temperature rise rate, and the second (main) ignition delay time, τ, as the timing of the second peak in temperature rise rate. For cases with single stage ignition there is only the main ignition delay time, τ.

τ_1 and τ are plotted over Z-space in Fig. 2 for T_{ox} values of 900, 1100, and 1300 K, which correspond to the intermediate temperature cases in this study and are expected to span the NTC regime. The 700 K results are not plotted (we did not observe autoignition at this temperature for the inlet velocity considered,

as will be discussed in section 4). The 1500 K results, also not shown, resemble the 1300 K results, but with a much shorter τ for lean Z, and two stage ignition is only observed for Z>0.4. The calculations were performed in a constant pressure, zero-dimensional reactor, using the solver SENKIN [28].

For each T_{ox}, two stage ignition is observed for Z values which have a mixture temperature (which is dependent on T_{ox} and Z) below 1100 K. τ_1 increases monotinically with Z from the point where first stage ignition is first observed (first stage ignition defined as a distinct peak in temperature rise rate, that preceeds the main stage of ignition), and the time interval between the first stage and main ignition decreases with Z, until the two stages merge at rich mixture fractions. Following early work on DNS of single stage ignition [29], a most reactive mixture fraction is defined for the first stage $Z_{mr,1}$ as the mixture having the shortest first stage ignition delay. Since τ_1 increases monotonically, $Z_{mr,1}$ corresponds to the lowest Z value for a given T_{ox} which produces a two stage ignition. The second stage ignition delay is non-monotonically dependent on Z and has one or two local minima. The non-monotonicity is a result of the NTC behaviour. Locally most reactive mixture fractions Z_{mr} can be defined for the main ignition as the mixture fractions corresponding to these local minima. The $Z_{mr,1}$ and Z_{mr} are given in Table 1. For the 700 K, 900 K and 1100 K cases, and the richer of the two local minima in the 1300 and 1500 K cases, the Z_{mr} are found in increasingly rich conditions as T_{ox} increases. This is due to the NTC behaviour and the fact that the fuel temperature (400 K) is much lower than the oxidiser temperature. For the 1300 K and 1500 K cases, the leaner of the two local minima (which are also the global minima) are found in increasingly lean conditions as T_{ox} increases, which is the expected behaviour for a positive temperature coefficient regime. Further discussion of the Z_{mr} in the 1300K and 1500K will only relate to the leaner of the two values.

4. Results

4.1. Flame structure

Figure 3 shows the heat release rate about the stabilisation point for each of the six cases. The image is oriented with the fuel side on the right. The stoichiometric mixture fraction contour (Z_{st}=0.1234) is superimposed by a solid line and, to help understand the divergence around the flame, and, to indicate the edge of the reactive region, the contour Z=0.01 is also shown by a dash-dot line. The star-shaped markers indicate the stabilisation point of the main ignition or flame as defined by the most upstream location with hydroxyl radical mass fraction, Y_{OH}, equal to 20% of the maximum value in the domain.

The square-shaped markers indicate the first stage autoignition kernel as defined by the most upstream location with $Y_{CH_3OCH_2O_2}$ (which is the key radical in R3) equal to 20% of the maximum value in the domain (these definitions were deemed appropriate as they produced consistent results for all cases). All cases have a stabilised flame, as judged by key species transport budgets (see section 4.2).

Figure 3 shows a transition in flame structure with variation in T_{ox}. At 700 K, the flame has a conventional tribrachial structure which has been studied extensively at atmospheric conditions. At 900 K, in addition to the main tribrachial structure there is a fourth, *upstream* branch, and this structure is termed tetrabrachial for its four branches. The 1100 K and 1300 K flames have a main tribrachial structure with two additional upstream branches, and so are termed pentabrachial. At 1500 K, the flame reverts to a tetrabrachial structure. The tetrabrachial and pentabrachial flames appear to combine features of conventional tribrachial flames and autoignition which, to the best of the authors' knowledge, have not been previously observed.

The location of the stabilisation point, $Z_{\bigstar}$, and the location of the initiation of first stage ignition, $Z_{\square}$, in mixture fraction space are compared to the $Z_{mr,1}$ and Z_{mr} values in Table 2. There is good correspondence between the location of the upstream branches in Z space and the $Z_{mr,1}$ and Z_{mr} values, and the trend of $Z_{mr,1}$ moving progressively to richer mixtures as T_{ox} is increased is well captured by the zero-dimensional model. This suggests that the upstream behaviour is due to autoignition (this will be further supported by the results in section 4.2). In the 900 K case, there is a single upstream heat release branch that is initiated near the $Z_{mr,1}$ value, suggesting that this branch is due to the first stage of ignition. Moving downstream, this upstream branch progressively moves towards richer mixtures and there is a decreasing distance between it and the main flame, which corresponds well to the dependence of the first stage ignition delay time and the dwell between ignitions that may be observed in the homogeneous reactor results in Fig. 2, which further supports the notion that this upstream branch has an autoignitive character. In the 1100 K case there are two upstream branches. The branch which is initiated far upstream at x = 0.7 mm, occurs near the $Z_{mr,1}$ value and so is identified with the first stage of ignition. The second, much shorter branch is initiated near Z_{mr} and so is due to the main ignition. In the 1300 K case there are two upstream branches, one in very lean and the other in very rich mixture fractions. The rich upstream branch is initiated near $Z_{mr,1}$ and is due to first stage ignition. The lean upstream branch is initiated at very lean mixture fractions near Z_{mr} and is due the main ignition. In the 1500 K case there is one upstream branch initiated near Z_{mr} due to the main ignition, and no first stage ignition is observed for

the given inlet velocity.

Overall, the complex transition in flame structure observed with variation in T_{ox} can be explained by the temperature dependent behaviour of the first and main stages of ignition. At 700 K the temperature is too low to activate first or main stage ignition for the given inlet velocity and residence time. For cases with T_{ox} of 900, 1100, 1300, and 1500 K, one or two upstream branches are observed. The upstream branches arise due to one of two possible scenarios: the first stage of ignition and are initiated from $Z_{mr,1}$ and then move to increasingly rich mixture fractions and eventually merge with the rich premixed branch downstream; or the main stage of ignition and are initiated near Z_{mr} and lead to the main ignition.

4.2. Transport budget analysis

Examining the contribution of transport and reaction in the species continuity equations provides a measure of the relative importance of spontaneous ignition versus deflagration. It has been used in previous studies to delineate different combustion modes, for example, to differentiate deflagrations where molecular transport is important (e.g. conduction from burned products to unburned reactants) from spontaneous autoignitions in which molecular transport is negligible [30–32]. Consider the transport equation for a given species, i, in Eq. (1):

$$\frac{\partial}{\partial t}\left[\rho Y_i\right] = -\frac{\partial}{\partial x_j}\left[\rho Y_i u_j\right] - \frac{\partial}{\partial x_j}\left[\rho Y_i V_{j,i}\right] + \omega_i, \tag{1}$$

where ρ is density, $V_{j,i}$ is the diffusion velocity, and ω_i is the species mass reaction rates.

For a steady solution, the left hand side (LHS) of Eq. (1) is zero. Equation (1) was evaluated for several key species and for all cases. The LHS in each case was found to be near zero (two orders of magnitude smaller than the largest term on the right hand side (RHS)), and so all of the simulations exhibit stabilised flames. A comparison of the terms on the RHS of Eq. (1) is made where the first term on the RHS represents convection, $\mathbf{C}$, the second term represents diffusion, which has $\hat{x}$ and $\hat{y}$ components $\mathbf{D}_x$ and $\mathbf{D}_y$, and the third term represents reaction, $\mathbf{R}$.

Line plots of the transport budget terms for species OH, evaluated for streamwise lines through the stabilisation point, are presented in Fig. 5. (Note that for clarity, it was necessary to use different scales on both axes for each sub-figure). A transition in the transport budget structure about the stabilisation point is observed. For the 700 K case, the formation and consumption of OH due to chemical reaction occurs

in a very thin region on the order of 0.01 mm and this is balanced by $\mathbf{D}_x$, with almost no contribution from **C**, which is consistent with the inner reaction layer of a premixed deflagrating flame. At 900 K, the transport budget is still dominated by $\mathbf{D}_x$ and **R**, but the **C** term becomes significant. For the 1100 (not shown here), 1300, and 1500 K cases, a transition to a **C**-**R** balance is observed and the **R** zone is more widely distributed spatially while $\mathbf{D}_x$ and $\mathbf{D}_y$ become small. The 1100 K, 1300 K and 1500 K cases are therefore identified as primarily spontaneous autoignition fronts, which propagate relative to the flow down a gradient of residence time. These results suggest that the transition from a propagating flame to autoignition is gradual and there is a broad temperature range where both modes are significant. Line plots of other radical species involved in high temperature reactions (not shown here) yield similar results.

In order to understand the behaviour of the first stage upstream heat release branch, a transport budget analysis was conducted for cross-stream lines in the 1300 K case for methoxymethyl-peroxy radical, $CH_3OCH_2O_2$ which is presented in Fig. 5. Far upstream of the stabilisation point, at x=0.84 mm, the balance is principally between **R** and **C**. This suggests that at this location the branch essentially is autoignitive. Further downstream, $\mathbf{D}_y$ becomes increasingly prominent, suggesting that the mode of burning in this branch develops a nonpremixed character.

5. Conclusions

With a view to understanding the possible importance of edge flames in lifted flame stabilisation in diesel engines, a suite of laminar edge flame DNS has been carried out in engine-relevant thermochemical conditions. At the considered conditions, the mixture ahead of the edge flame can autoignite given sufficient residence time, which introduces different behaviours compared with edge flames at atmospheric conditions.

DME was selected as the fuel as a representative bio-alcohol with a manageably sized chemical kinetic mechanism but still represents important features of diesel fuel, namely two stage autoignition and NTC regime. A parametric study was performed varying the ambient temperature. Five cases were considered at 700, 900, 1100, 1300, and 1500 K at a fixed pressure of 40 atm.

For the 700 K case, a conventional tribrachial edge flame was observed, similar to flames that have been previously studied at atmospheric conditions.

For cases 900, 1100, 1300, and 1500 K, new flame structures were observed. These flames exhibit a tribrachial main flame structure similar to that observed at atmospheric conditions, with a crescent-shaped premixed combustion region and a trailing diffusion flame. However, unlike edge flames in atmospheric

conditions, the flames exhibit additional upstream branches due to autoignition, such that the flames are either tetrabrachial or pentabrachial. Cases 900, 1100, and 1300 K exhibit a low temperature upstream branch. The cases with 1100, 1300, and 1500 K oxidiser temperature exhibit a high temperature upstream branch, which occurrs on the rich side at 1100 K and on the lean side at 1300 and 1500 K.

The existence and location in mixture fraction space of the low and high temperature upstream branches was found to be controlled by the temperature and mixture fraction dependent behaviour of the first- and second stage ignitions. For a given inlet velocity and thermochemical condition, low and high temperature upstream branches exist if their first- and second stage ignition delay times are sufficiently short such that they may develop ahead of the main tribrachial flame.

The stabilisation mechanism was found to be temperature dependent, with the 1100, 1300, and 1500 K cases propagating at high velocity and being stabilised essentially by autoignition while for the 700 and 900 K cases, the velocity was more modest and the flame appeared to be stabilised by premixed flame propagation.

The results suggest that even in autoignitive conditions, essentially premixed edge-flame structures or hybrid premixed-autoignition structures can occur, and these could therefore contribute to the stabilisation of lifted flames in diesel engines. Further work is needed to understand how these structures are affected by a number of parameters including velocity, mixing layer thickness, shear, and turbulence.

Acknowledgements

This work was supported by the Australian Research Council (ARC). The work at Sandia National Laboratories was supported by the Combustion Energy Frontier Research Center, an Energy Frontier Research Center funded by the US Department of Energy (DOE), Office of Science, Office of Basic Energy Sciences under Award No. DE-SC0001198. Sandia is a multiprogram laboratory operated by Sandia Corporation, a Lockheed Martin Company, for the United States Department of Energy under contract DE-AC04-94AL85000. The research was also supported by computational resources on the Australian NCI National Facility through the National Computational Merit Allocation Scheme and Intersect Australia partner share.

6. References

[1] J. Buckmaster, Prog. Energ. Combust. Sci. 28 (2002) 435–475.

[2] S.H. Chung, Proc. Combust. Inst. 31 (2007) 877–892.

[3] N.I. Kim, J.I. Seo, K.C. Oh, H.D. Shin, Proc. Combust. Inst. 30 (2005) 367 – 374.

[4] J. Daou, A. Liñán, Proc. Combust. Inst. 27 (1998) 667 – 674.

[5] Y.S. Ko, S.H. Chung, Combust. Flame 118 (1999) 151 – 163.

[6] J.I. Seo, N.I. Kim, H.D. Shin, Combust. Flame 153 (2008) 355 – 366.

[7] P. Kioni, B. Rogg, K. Bray, A. Liñán, Combust. Flame 95 (1993) 276 – 290.

[8] H.G. Im, J.H. Chen, Combust. Flame 119 (1999) 436–454.

[9] H.G. Im, J.H. Chen, Combust. Flame 126 (2001) 1384 – 1392.

[10] T. Echekki, J.H. Chen, Combust. Flame 114 (1998) 231–245.

[11] D. Siebers, B. Higgins, L. Pickett, SAE Paper 2002-01-0890 (2002).

[12] H. Ciezki, G. Adomeit, Combust. Flame 93 (1993) 421 – 433.

[13] Y. Wang, C.J. Rutland, Combust. Flame 149 (2007) 353 – 365.

[14] J.H. Chen, A. Choudhary, B. de Supinski, M. DeVries, E.R. Hawkes, S. Klasky, W.K. Liao, K.L. Ma, J. Mellor-Crummey, N. Podhorszki, R. Sankaran, S. Shende, C.S. Yoo, Comp. Sci. Disc. 2 (2009) 015001.

[15] T. Poinsot, S. Lele, J. Comp. Phys. 101 (1992) 104 – 129.

[16] H. Zhang, E.R. Hawkes, J.H. Chen, S. Kook, Proc. Combust. Inst. 34 (2013) 803 – 812.

[17] O. Chatakonda, E.R. Hawkes, A.J. Aspden, A.R. Kerstein, H. Kolla, J.H. Chen, Combust. Flame 160 (2013) 2422 – 2433.

[18] E.R. Hawkes, O. Chatakonda, H. Kolla, A.R. Kerstein, J.H. Chen, Combust. Flame 159 (2012) 2690 – 2703.

[19] R. Sankaran, E.R. Hawkes, J.H. Chen, T. Lu, C.K. Law, J. Phys.: Conf. Ser. 46 (2012) 38 – 42.

[20] A. Gruber, R. Sankaran, E.R. Hawkes, J.H. Chen, J. Fluid Mech. 658 (2010) 5–32.

[21] E.R. Hawkes, R. Sankaran, J.H. Chen, S.A. Kaiser, J.H. Frank, Proc. Combust. Inst. 32 (2009) 1455 – 1463.

[22] T. Lu, Personal communication (2013).

[23] Z. Zhao, M. Chaos, A. Kazakov, F.L. Dryer, Int. J. Chem. Kinet. 40 (2008) 1–18.

[24] T. Lu, C.K. Law, Prog. Energ. Combust. Sci. 35 (2009) 192 – 215.

[25] H.J. Curran, W.J. Pitz, C.K. Westbrook, P. Dagaut, J.C. Boettner, M. Cathonnet, Int. J. Chem. Kinet. 30 (1998) 229–241.

[26] H.J. Curran, S.L. Fischer, F.L. Dryer, Int. J. Chem. Kinet. 32 (2000) 741–759.

[27] X.L. Zheng, T.F. Lu, C.K. Law, C.K. Westbrook, H.J. Curran, Proc. Combust. Inst. 30 (2005) 1101–1109.

[28] A.E. Lutz, R.J. Kee, J.A. Miller, Sandia National Laboratories Report No. SAND87-8248 (2002).

[29] C. Markides, E. Mastorakos, Proc. Combust. Inst. 30 (2005) 883 – 891.

[30] J.H. Chen, E.R. Hawkes, R. Sankaran, S.D. Mason, H.G. Im, Combust. Flame 145 (2006) 128 – 144.

[31] C.S. Yoo, H.G. Im, Proc. Combust. Inst. 31 (2007) 701 – 708.

[32] R.L. Gordon, A.R. Masri, S.B. Pope, G.M. Goldin, Combust. Flame 151 (2007) 495 – 511.

Table 1: Values of variable parameters for each case.

Case	T_{ox} [K]	U [ms^{-1}]
1	700	1.25
2	900	3.50
3	1100	5.75
4	1300	10.00
5	1500	45.00

Table 2: Location in mixture fraction space of the star and square shaped markers from Fig. 3 compared to the $Z_{mr,1}$ and Z_{mr} values from the zero-dimensional simualtions. $Z_{\bigstar}$ corresponds to the stabilisation point and $Z_{\square}$ corresponds to the point where the first stage ignition first develops.

T_{ox} [K]	$Z_{mr,1}$	$Z_{\square}$	Z_{mr}	$Z_{\bigstar}$
700	0.03	-	0.05	0.12
900	0.03	0.04	0.11	0.13
1100	0.15	0.16	0.21	0.18
1300	0.27	0.31	0.05, 0.33	0.06
1500	0.35	-	0.01, 0.39	0.04

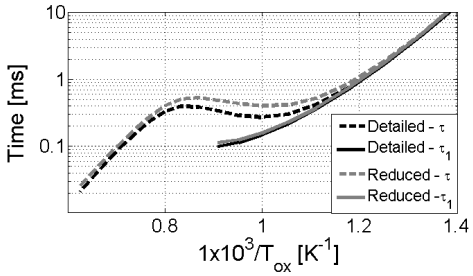

Figure 1: Comparison of first (τ_1) and main (τ) stage ignition delay times for the detailed and reduced dimethyl ethere chemical mechanisms.

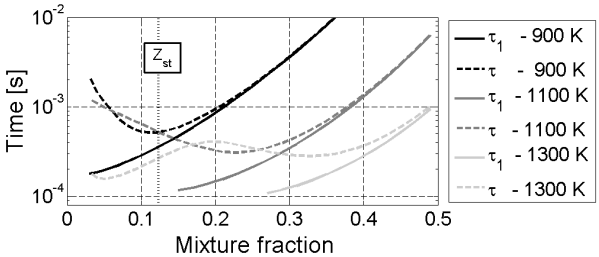

Figure 2: τ_1 and τ over Z-space for various T_{ox}.

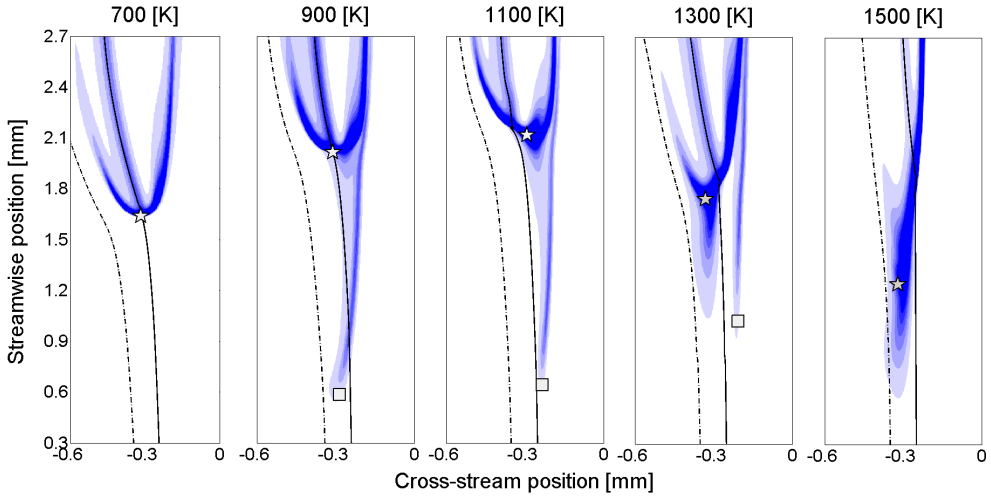

Figure 3: Colour shadings show the heat release rate field. The maximum value of the colour shading is -1×10^{12} in cases 700 and 900 K, -1.5×10^{12} in cases 1100 and 1300 K, and -4×10^{12} in case 1500 K, with units of [Jm^{-3}s^{-}1]. The solid line indicates the Z_{st} contour, the dashed line indicates the contour Z = 0.01. The star-shaped markers indicate the location of the stabilisation point. The square-shaped markers indicate the location on the first stage autoignition kernel.

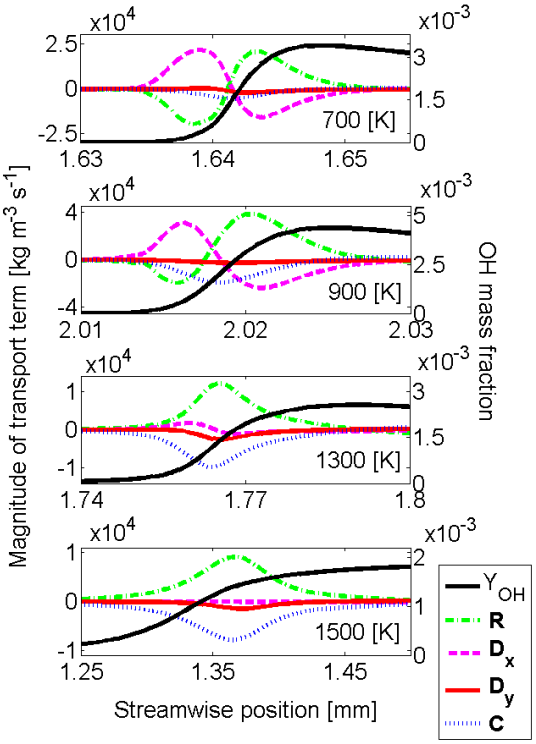

Figure 4: Transport budget analysis and mass fraction profile for species OH. Subfigures present streamwise line evaluations through the stabilisation point for each case, ordered by increasing T_{ox} from top to bottom.

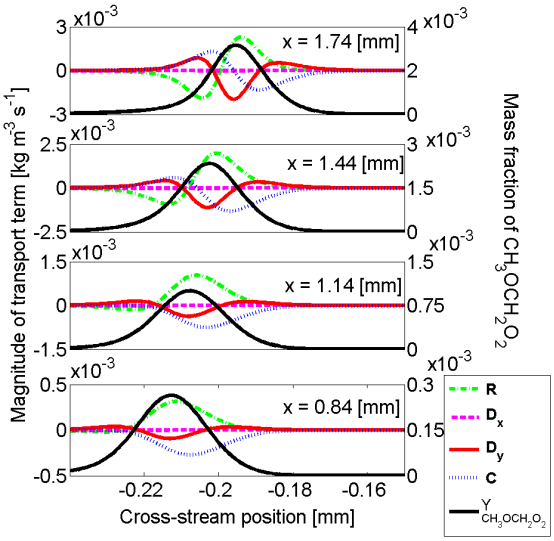

Figure 5: Transport budget analysis and mass fraction profile for species $CH_3OCH_2O_2$ in case with T_{ox} of 1300 K. Subfigures are cross-stream line evaluations at intervals of 0.3 [mm] starting at the stabilisation point (top subfigure).

List of Figures